3

Separation of Carbon Dioxide from Flue Gas Using Adsorption on Porous Solids

Tirzhá L. P. Dantas[1], Alírio E. Rodrigues[2] and Regina F. P. M. Moreira[3]
[1]*Federal University of Paraná, Department of Chemical Engineering*
[2]*University of Porto, Faculty of Engineering*
[3]*Federal University of de Santa Catarina, Department of Chemical and Food Engineering*
[1,3]*Brazil*
[2]*Portugal*

1. Introduction

The generation of CO_2 is inherent in the combustion of fossil fuels, and the efficient capture of CO_2 from industrial operations is regarded as an important strategy through which to achieve a significant reduction in atmospheric CO_2 levels. There are three basic CO_2 capture routes: (1) pre-combustion capture (via oxygen-blown gasification); (2) oxy-fuel combustion, i.e. removing nitrogen before combustion; and (3) post-combustion capture.

Adopting the post-combustion capture route avoids the potentially long time periods required to develop cost-effective coal-derived syngas separation technologies, hydrogen turbine technology, and fuel-cell technology, etc. It can also provide a means of CO_2 capture in the near-term for new and existing stationary fossil fuel-fired power plants.

Concentrations of CO_2 in power station flue gases range from around 4% by volume for natural gas combined cycle (NGCC) plants to 14% for pulverized fuel-fired plants. In the carbon capture and storage chain (capture, transport and storage) different requirements have been set for the composition of the gas stream mainly containing CO_2, which can vary within the range of 95-97% CO_2 with less than 4% N_2.

There are several post-combustion gas separation and capture technologies currently being investigated, namely: (a) absorption, (b) cryogenic separation, (c) membrane separation, (d) micro-algal bio-fixation, and (e) adsorption.

Current absorption technologies which propose the capture of CO_2 from flue gas are costly and energy intensive. Membrane technology is an attractive CO_2 capture option because of advantages such as energy-efficient passive operation, no use of hazardous chemicals, and tolerance to acid gases and oxygen. However, an important challenge associated with membrane technology is how to create the driving force efficiently, because the feed flue gas is at ambient pressure and contains a relatively low CO_2 content.

Solid sorbents are another promising capture technology. These sorbents can either react with the CO_2 or it can be adsorbed onto the surface. Chemical sorbents that react with the

CO_2 in the flue gas can be comprised of a support, usually of high surface area, with an immobilized amine or other reactant on the surface. Physical adsorbents can separate the CO_2 from the other flue gas constituents, but do not react with it. Instead, they use their cage-like structure to act as molecular sieves. These sorbents can be regenerated using a pressure swing or a temperature swing, although the costs associated with a pressure swing may be prohibitively high. Physisorbents such as activated carbon and zeolites will be safe for the local environment, and are generally relatively inexpensive to manufacture. Conventionally, activated carbon materials have been widely applied in industry for gas separation, and also have been investigated for CO_2 capture. Carbon dioxide emissions are frequently associated with large amounts of nitrogen gas, and thus an adsorbent selective to one of these compounds is required. These adsorbents should also be selective even at high temperatures, i.e., temperatures typical of carbon dioxide emission sources. Activated carbon is a suitable adsorbent and its CO_2 adsorption characteristics are dependent on its surface area and chemical surface characteristics. The surface chemistry of activated carbon is determined by the amount and type of heteroatom, for example oxygen, nitrogen, etc. Therefore, the adsorption capacity of activated carbon for carbon dioxide is a function of its pore structure and the properties of the surface chemistry.

Strategies like PSA (pressure swing adsorption), TSA (temperature swing adsorption) and ESA (electric swing adsorption) processes have been proposed and investigated for adsorption in a cyclic process (Cavenati *et al*., 2006; Grande & Rodrigues, 2008; Zhang et al., 2008). PSA is a cyclical process of adsorption/desorption that occurs through pressure changes and can be very suitable for carbon dioxide separation from exhaust gases due to its easy application in a large temperature range. The most studies presents the CO_2/N_2 separation using PSA process at room temperature, but it has been reported that is possible to obtain high purity CO_2 (~90%) at high temperature (Ko *et al*., 2005). Recently, Grande and Rodrigues (2008) reported that it is possible to recover around 89% of the CO_2 from a CO_2/N_2 mixture using honeycomb monoliths of activated carbon through ESA. However, the temperature of the CO_2/N_2 mixture in a typical exhaust gas can exceed 100°C and at such temperatures the recovery and purity of CO_2 can be significantly modified.

2. Experimental section

2.1 Selection and preparation of adsorbents

The commercial activated carbon used was Norit R2030 (Norit, Netherlands) which was selected due to its high adsorption capacity for CO_2. The nitrogen-enriched activated carbon, denoted as CPHCL, was prepared in a way similar way to that as previously reported (Gray et al., 2004), mixing 10 g of activated carbon with 500mL of 10^{-1}M 3-chloropropylamine hydrochloride solution. The mixture was kept under constant stirring, at ambient temperature for 5 hours. The CPHCL adsorbent was then left to dry for 12 hours in an oven at 105°C.

2.2 Characterization of the adsorbents

The content of carbon, hydrogen and nitrogen was determined by elemental analysis using CHNS EA1100 equipment (CE Instruments, Italy).

Thermogravimetric experiments were carried out with a TGA-50 thermogravimetric analyzer (Shimadzu, Japan) in the temperature range of 30°C – 900°C, at a heating rate of 10°C /min under nitrogen flow.

Fourier transform infrared (FTIR) spectroscopy was used to qualitatively identify the chemical functionality of activated carbon. To obtain the observable adsorption spectra, the solids were grounded to an average diameter of ca. 0.5 mm. The transmission spectra of the samples were recorded using KBr pellets containing 0.1% of carbon. The pellets were 12.7mm in diameter and ca. 1mm thick and were prepared in a manual hydraulic press set at 10 ton. The spectra were measured from 4000 to 400 cm^{-1} and recorded on a 16PC FTIR spectrometer (Perkin Elmer, USA).

X-ray photoelectron spectroscopy (XPS) measurements were carried out with a VG Microtech ESCA3000 MULTILAB spectrometer using monochromatic Al Ka X-rays. The pass energy of the analyzer was 58.7 eV for high-resolution scans. Relative elemental concentrations on the surface of the sorbents were calculated by measuring peak areas in the

high-resolution spectra and then converting to atomic concentrations using sensitivity factors provided by the instrument manufacturer.

2.3 Adsorption equilibrium isotherms

The equilibrium of CO_2 and N_2 adsorption on activated carbon was measured at different temperatures of 30°C, 50°C, 100°C, and 150°C using the static method in a Rubotherm magnetic suspension microbalance (Bochum, Germany) up to approximately 5 bar.

The equilibrium of CO_2 adsorption on CPHCL was measured at different temperatures of 30°C, 50°C, 100°C, and 150°C by the volumetric method, in an automatic sorptometer, Autosorb 1C (Quantachome, USA), up to approximately 1 bar.

Before the adsorption measurements, the solid samples were pre-treated for 12 hours at 150°C under vacuum. This temperature ensures that the amine is homogeneously tethered to the solid surface without devolatilize or decompose it.

2.4 Breakthrough curves: Fixed-bed CO_2 adsorption and CO_2/N_2 mixture adsorption

All the experimental breakthrough curves were obtained by passing the appropriate gas mixture through the packed column with the adsorbent: activated carbon or CPHCL. The solid adsorbent was pre-treated by passing helium at a flow rate of 30 $mL.min^{-1}$ n and at 150°C for 2 hours. These breakthrough curves were obtained 30°C, 50°C, 100°C, and 150°C.

The dynamic of adsorption of CO_2 in a fixed bed was studied using CO_2 diluted in helium (CO_2/He = 20%/80% v/v) in order to obtain the breakthrough curves. For the fixed-bed CO_2/N_2 separation dynamics, the breakthrough curves were obtained by passing the standard gas mixture – 20% CO_2/ 80%N_2 v/v.

The total gas flow rate was maintained at 30 $mL.min^{-1}$ which was controlled by a mass flow unit (Matheson, USA). The column was located inside a furnace with controlled temperature. A gas chromatographic model CG35 (CG Instrumentos Científicos, Brazil) equipped with a Porapak-N packed column (Cromacon, Brazil) and with a thermal

conductivity detector (TCD) was used to monitor the carbon dioxide or nitrogen concentration at the bed exit, using helium as the reference gas. The experimental system – column and furnace – was considered adiabatic because it was isolated with a layer of 0.10m of fiber glass and with a refractory material. The characteristics of the fixed bed and the column are presented in Table 1

	CO_2 and CO_2/N_2 adsorption in a fixed bed [a]	PSA experiments [b]
Bed length, L	0.171 m	0.83 m
Bed diameter, d_{int}	0.022 m	0.021 m
Bed weight, W	0.0352 kg	0.158 kg
Bed voidage fraction, ε	0.52	0.52
Column wall thickness, l	0.0015m	0.0041m
Column wall specific heat, $C_{p,w}$	440 J $kg^{-1}K^{-1}$	500 J $kg^{-1}K^{-1}$
Column wall conductivity, k_w		1.4 W $m^{-1}K^{-1}$
Wall density, ρ_w	7280 kg m^{-3}	8238 kg m^{-3}

Table 1. Characteristics of the fixed bed and the column used in the experiments [[a] Dantas *et al*., 2010; [b] Dantas *et al*., 2011].

2.5 Pressure swing adsorption

The PSA experimental setup consisted of one fixed-bed adsorption that simulated the operation of a unit with several fixed-beds, for which more details are given elsewhere (Da Silva & Rodrigues, 2001). The solid adsorbent used was the commercial activated carbon which was pre-treated by passing helium at a flow rate of 1.0 L.min^{-1} and at 150°C for 12 hours. The PSA experiments were performed premixed CO_2 to N_2 forming a mixture - 0.15 v/v. The flow rate of each gas was controlled by mass controllers (Teledyne Brown Engineering, USA).

A gas chromatographic model CP9001 (Chrompack 9001, Netherlands) equipped with a Poraplot Q capillary column (Varian, Netherlands), with a thermal conductivity detector (TCD), and with a flame ionization detector (FID) was used to monitor the carbon dioxide or nitrogen concentration at the bed exit, using helium as the reference gas. The experimental system – column and furnace – was considered adiabatic because it was isolated with a layer of 0.10m of fiber glass and with a refractory material. The temperature inside the column was continuously monitored using a K-thermocouple placed at 0.17 m and 0.43 m from the bottom of the column. The column was located inside a convective furnace and thus the system was considered to be non-adiabatic. The characteristics of the fixed bed and the column are presented in Table 1.

The cycles were of the Sharstrom-cycle type and divided by pressurization with pure nitrogen at a flow rate of 3.0 L.min^{-1}, feeding at constant pressure of 1.3 bar and total flow rate of 3.0 L.min^{-1}, countercurrent blowdown decreasing the pressure to 0.1bar and

countercurrent purge with pure nitrogen at constant pressure and a flow rate of 0.5 L.min^{-1}. All experiments were performed with 20 seconds of pressurization and 70 seconds of depressurization. However, different feed and purge times were used. Table 2 summarizes the PSA experimental conditions used in this study.

Run	T, °C	Feed Time, s	Purge time, s
1	50	100	70
2	50	120	50
3	100	120	50
4	100	200	50

Table 2. PSA experimental conditions.

2.5.1 Performance criteria of the PSA process

The definition of the performance criteria provides a common basis for comparing the different experiments. These are; Eq (1) to (3):

$$\text{Purity of } CO_2 = \frac{\int_{t_{blowdown}}^{t_{purge}} F_{CO_2}\,dt}{\sum_{i=1}^{n_{comp}} \int_{t_{blowdown}}^{t_{purge}} F_i\,dt} \tag{1}$$

$$\text{Purity of } N_2 = \frac{\int_{t_{blowdown}}^{t_{purge}} F_{N_2}\,dt}{\sum_{i=1}^{n_{comp}} \int_{t_{blowdown}}^{t_{purge}} F_i\,dt} \tag{2}$$

$$\text{Recovery of } CO_2 = \frac{\int_{t_{blowdown}}^{t_{purge}} F_{CO_2}\,dt}{\int_{0}^{t_{purge}} F_{CO_2}\,dt} \tag{3}$$

where F_i is the molar flow rate of component i – carbon dioxide or nitrogen.

3. Mathematical modelling

3.1 Model description

The model used to describe the fixed-bed experiments is derived from the mass, energy and momentum balances. The flow pattern is described with the axially dispersed plug flow model and the mass transfer rate is represented by a Linear Driving Force model – LDF. It was assumed that the gas phase behaves as an ideal gas and the radial concentration and

temperature gradients are negligible. The fixed-bed model is described by the equations given below.

The mass balance for each component is given by Eq. (4); (Ruthven, 1984):

$$\varepsilon \frac{\partial C_i}{\partial t} + \frac{\partial (uC_i)}{\partial z} = \varepsilon D_L \frac{\partial^2 C_i}{\partial z^2} - (1-\varepsilon)\rho_p \frac{\partial \overline{q}_i}{\partial t} \tag{4}$$

where ε is the bed void fraction, C_i is the gas phase concentration of component *i*, $\overline{q}_i$ is the average amount of component i adsorbed, D_L is the axial mass dispersion coefficient, u is the superficial velocity, and ρ_p is the particle density.

The rate of mass transfer to the particle for each component is given by Eq. (5):

$$\frac{\partial \overline{q_i}}{\partial t} = K_{L,i}(q_i^* - \overline{q}_i) \tag{5}$$

where K_L is the overall mass transfer coefficient of component i and q_i^* is the amount adsorbed at equilibrium, i.e., $q_i^* = f(C_i, T_g)$ given by the adsorption isotherm, and $\overline{q}_i$ is the average amount adsorbed.

The concentration C_i is given by Eq (6):

$$C_i = \frac{y_i P}{RT_g} \tag{6}$$

where y_i is the molar fraction of each gas in the gas phase, P is the total pressure, T_g is the gas temperature and R is the universal gas constant.

The Ergun equation considers the terms for the pressure drop and velocity changes; Eq. (7):

$$-\frac{\partial P}{\partial z} = 150\frac{\mu_g (1-\varepsilon)^2}{\varepsilon^3 {d_p}^2} u + \ 1.75\frac{(1-\varepsilon)}{\varepsilon^3 d_p}\rho_g u^2 \tag{7}$$

where μ_g is the gas viscosity, ρ_g is the gas density, and d_p is the particle diameter.

The energy balance is; Eq. (8):

$$\begin{aligned} &\varepsilon C C_{v,g}\frac{\partial T_g}{\partial t} + C C_{p,g}\frac{\partial (uT_g)}{\partial z} = \varepsilon \lambda_L \frac{\partial^2 T_g}{\partial z^2} - \\ &-(1-\varepsilon)\rho_p C_s \frac{\partial T_s}{\partial t} + \ (1-\varepsilon)\rho_p \sum_i \left(-\Delta H_i\right)\frac{\partial \overline{q_i}}{\partial t} - \frac{4h_w}{d_{\text{int}}}(T_g - T_w) \end{aligned} \tag{8}$$

where $C_{v,g}$ is the molar specific heat at constant volume for the gas phase, $C_{p,g}$ is the molar specific heat at constant pressure for the gas phase, λ_L is the axial heat dispersion coefficient, C_s is the solid specific heat, $\left(-\Delta H_i\right)$ is the heat of adsorption for component i at zero coverage, h_w is coefficient for the internal convective heat transfer between the gas and the column wall, d_{int} is the bed diameter, and T_w is the wall temperature.

The solid phase energy balance is expressed by Eq. (9):

$$\rho_p C_s \frac{\partial T_s}{\partial t} = \frac{6h_f}{d_p}(T_g - T_s) + \rho_p \sum_i \left(-\Delta H_i\right) \frac{\partial \overline{q_i}}{\partial t} \tag{9}$$

where h_f is the coefficient for film heat transfer between the gas and the adsorbent.

For the column wall, the energy balance can be expressed by Eq. (10) to (12):

$$\rho_w C_{p,w} \frac{\partial T_w}{\partial t} = \alpha_w h_w (T_g - T_w) - \alpha_{wl} U (T_w - T_\infty) \tag{10}$$

with

$$\alpha_w = \frac{d_{\text{int}}}{l\left(d_{\text{int}} + l\right)} \tag{11}$$

and

$$\alpha_{wl} = \frac{d_{\text{int}}}{\left(d_{\text{int}} + l\right) \ln\left(\frac{d_{\text{int}} + l}{d_{\text{int}}}\right)} \tag{12}$$

where ρ_w is the column wall density, $C_{p,w}$ is the column wall specific heat, α_w is the ratio of the internal surface area to the volume of the column wall, α_{wl} is the ratio of the logarithmic mean surface area of the column shell to the volume of the column (Cavenati *et al.*, 2006), U is the external overall heat transfer coefficient, and T_∞ is the furnace external air temperature. For an adiabatic system, the last term of this equation must not been considered.

3.2 Boundary and initial conditions

The mathematical model was solved using the commercial software gPROMS (Process System Enterprise Limited, UK) which uses the method of orthogonal collocation on finite elements for resolution. The boundary and initial conditions were the show bellow.

3.2.1 For the breakthrough curves

The initial conditions for the adiabatic system are:

$$T_w = T_g = T_s = T_i \;;\; P = P_0 \;\text{ and }\; C_i(z,0) = \overline{q}_i(z,0) = 0 \tag{13}$$

The boundary conditions are described by the equations given below (Eq.14-18).

1. Bed inlet: (z=0)

$$\varepsilon D_L . \left.\frac{\partial C_i}{\partial z}\right|_{z^+} = -u\left(C_i\big|_{z^-} - C_i\big|_{z^+}\right) \tag{14}$$

$$\varepsilon\lambda_L.\left.\frac{\partial T_g}{\partial z}\right|_{z^+} = -uCC_{p,g}(T_g|_{z^-} - T_g|_{z^+}) \tag{15}$$

$$uC|_{z^-} = uC|_{z^+} \tag{16}$$

2. Bed outlet: (z=L)

$$\left.\frac{\partial C_i}{\partial z}\right|_{z^-} = 0 \tag{17}$$

$$\left.\frac{\partial T_g}{\partial z}\right|_{z^-} = 0 \tag{18}$$

3.2.2 For PSA experiments

The initial conditions, only considered for the unused bed, are:

$$T_w = T_g = T_s = T_0 \; ; P = P_0 \;\text{ and }\; C_i(z,0) = \overline{q}_i(z,0) = 0 \tag{19}$$

The initial condition of each new cycle corresponds to the final condition of the previous cycle. The boundary conditions for the mass and energy balances are described by the equations given below (Eq.20-27).

1. Bed inlet: pressurization step (z=0), feed step (z=0) and countercurrent purge step (z=L).

$$\varepsilon D_L \left.\frac{\partial C_i}{\partial z}\right|_{z^+} = -u(C_i|_{z^-} - C_i|_{z^+}) \tag{20}$$

$$\varepsilon\lambda_L.\left.\frac{\partial T_g}{\partial z}\right|_{z^+} = -uC_{p,g}(T_g|_{z^-} - T_g|_{z^+}) \tag{21}$$

2. Bed outlet: pressurization step (z=L), feed step (z=L), countercurrent purge step (z=0), and bed inlet and outlet for countercurrent blowdown step (z=L and z=0, respectively).

$$\left.\frac{\partial C_i}{\partial z}\right|_{z^-} = 0 \tag{22}$$

$$\left.\frac{\partial T_g}{\partial z}\right|_{z^-} = 0 \tag{23}$$

The boundary conditions for the momentum balance are the following:

1. Bed inlet: pressurization step (z=0).

$$P_{z^+} = P_{feed} \tag{24}$$

2. Bed outlet for pressurization step (z=L), and bed inlet for countercurrent blowdown step (z=L).

$$u\big|_{z^-} = 0 \tag{25}$$

3. Bed inlet: feed step (z=0), and countercurrent purge step (z=L).

$$u\big|_{z^-} = u\big|_{z^+} \tag{26}$$

4. Bed outlet: countercurrent blowdown step (z=0), and countercurrent purge step (z=0).

$$P\big|_{z^-} = P_{purge} \tag{27}$$

3.3 LDF global mass transfer coefficient and correlations used to estimation of model parameters

Table 3 summarizes the experimental conditions of temperatures and Reynolds numbers in Runs 1 - 4.

Table 4 shows the LDF global mass transfer coefficient, the axial dispersion coefficient, and the film mass transfer coefficient, should be evaluated using different correlations due different Reynolds numbers in Runs 1 -4 under adiabatic or non-adiabatic systems.

For the all experiments performed at adiabatic system – low Reynols number, the value of the LDF global mass transfer coefficient was estimated using the expression proposed by Farooq and Ruthven (1990) which considers all of the resistances to the mass transfer, i.e., intra- and extraparticle resistances; Eq. (28):

$$\frac{1}{K_L} = \frac{r_p q_o}{3k_f C_o} + \frac{{r_p}^2 q_o}{15\varepsilon_p D_e C_o} + \frac{{r_c}^2}{15D_c} \tag{28}$$

where r_p is the particle radius, k_f the external mass transfer coefficient, q_o the value of q at equilibrium with C_o (adsorbate concentration in the feed at feed temperature T_o and expressed in suitable units), ε_P the particle porosity, r_c the radius of activated carbon crystal and D_C is the micropore diffusivity. The micropore diffusivity values were those reported by Cavenati and coworkers (2006) since the micropore distribution of the adsorbents are similar to those of carbon molecular sieves (Cavenati *et al.*, 2006; Vinu & Hartmann, 2005).

For the all experiments performed at non-adiabatic system – high Reynols number, the value of the LDF global mass transfer coefficient was estimated that intraparticke resistance is only controlled by molecular diffusion.

All others correlations used to evaluate the mass and heat transport parameters are summarized in Table 4. The gas phase viscosity was estimated using Wilkes's equation (Bird *et al*., 2007). The axial mass dispersion coefficient (D_L), for the adiabatic system, was evaluated by Leitão & Rodrigues (1995); for the non-adiabatic system, according to Wakao and coworkers (1978). The film mass transfer coefficient (k_f), for the adiabatic system, was evaluated by Seguin et al. (1995); for the non-adiabatic system, according to Wakao and Funazkri (1978). The axial heat dispersion coefficient (λ_L) and the film heat transfer coefficient (h_f) were evaluated by

Wakao and coworkers (1978); the convective heat transfer coefficient between the gas phase and the column wall (h_w) was evaluated according to De Wash & Froment (1972).

		Run	T, °C	Re
Adiabatic System	CO_2 /He	1	28	0.12
		2	50	0.10
		3	100	0.08
		4	150	0.06
Adiabatic System	CO_2 /N_2	1	28	0.36
		2	50	0.32
		3	100	0.25
		4	150	0.20
Non-adiabatic System	PSA	1	50	41.64
		2	50	41.64
		3	100	32.31
		4	100	32.31

Table 3. Experimental conditions of temperature and Reynolds number.

Coefficient	Adiabatic system	Non-adiabatic system
Axial Mass Dispersion	$Pe = 0.508\,\mathrm{Re}^{0.020}\,\frac{L}{d_p}$	$\varepsilon\frac{D_L}{D_m} = 20 + 0.5Sc\,\mathrm{Re}$
Film mass transfer	$Sh = 1.09\,\mathrm{Re}^{0.27}\,Sc^{1/3}$	$Sh = 2 + 1.1\,\mathrm{Re}^{0.27}\,Sc^{1/3}$
Axial Heat Dispersion	$\frac{\lambda_L}{k_g} = 10 + 0.5\,\mathrm{Pr}\,\mathrm{Re}$	
Film heat transfer	$Nu = 2.0 + 1.1\,\mathrm{Re}^{0.6}\,\mathrm{Pr}^{1/3}$	
Internal convective heat transfer	$\frac{h_w d_{\mathrm{int}}}{k_g} = 12.5 + 0.048\,\mathrm{Re}$	
Global heat transfer	$U = \frac{1}{\frac{1}{h_w} + \frac{d_{\mathrm{int}}}{k_w}\ln\left(\frac{d_{ext}}{d_{\mathrm{int}}}\right) + \frac{d_{\mathrm{int}}}{d_{ext}}\frac{1}{h_{ext}}}$	
External convective heat transfer	$\frac{h_{ext}L}{k_{ext}} = 0.68 + \frac{0.67\,Ra^{1/4}}{\left[1+\left(\frac{0.492}{\mathrm{Pr}}\right)^{9/12}\right]^{4/9}}$	
$Pe = \frac{uL}{D_L}$; $\mathrm{Re} = \frac{\rho_g u d_p}{\mu_g}$; $Sc = \frac{\mu_g}{\rho_g D_m}$; $Sh = \frac{k_f d_p}{D_m}$; $\mathrm{Pr} = \frac{C_{p,g}\mu_g}{k_g}$; $Nu = \frac{h_f d_p}{k_g}$; $Ra = g\beta\frac{(T_w - T_\infty)}{\nu\alpha}L^3$		

Table 4. Correlations used for estimation of mass and heat parameters [Dantas *et al.*, 2011].

The effective diffusivities were calculated by Bosanquet equation and the molecular diffusivities were calculated with the Chapman-Enskong equation (Bird *et al*., 2007). A tortuosity of 2.2 and 1.8 was admitted to the activated carbon particle and CPHCL, respectively.

4. Results and discussion

4.1 Characterization of adsorbents

Textural properties of activated carbon and CPHCL were previously described (Dantas *et al*., 2010). The adsorbents are microporous and the BET surface areas are shown in Table 5.

Modifications with nitrogen-containing species may also result in changes in the porous structure (Arenilas *et al*., 2005). The CPHCL had a lower BET area when compared to the commercial activated carbon. The micropores volume of the CPHCL decreases considerably compared with the commercial activated carbon, suggesting that the nitrogen incorporation partially blocks the access of N_2 to the small pores.

The chemical characteristics of the adsorbents are given in Table 6. As expected, the adsorbent CPHCL has the greater nitrogen content and an N/C atomic ratio which is twice that of the commercial activated carbon.

The FTIR spectra of commercial activated carbon and CPHCL are shown in Figure 1. All spectra show the contribution from ambient water (at about 3600 cm^{-1}) and carbon dioxide (doublet at 2360 cm^{-1} and sharp spike at 667 cm^{-1}) present in the optical bench. The band of O-H stretching vibrations (3600 - 3100 cm^{-1}) was due to surface hydroxyl groups and chemisorbed water. The band at 2844 and 2925 cm^{-1} is frequently ascribed to the C–H stretching. The asymmetry of the band at 3600 – 3100 cm^{-1} indicates the presence of strong hydrogen bonds.

	Commercial activated carbon	**CPHCL**
S_{BET}, m^2/g	1053.0	664.6
S_{micro}, m^2/g	1343.0	753.0
V_{micro}, cm^3/g	0.0972	0.0388
Mean pore radius r_o , nm	1.23	1.54
Particle porosity ε_p	0.47	0.37
N_2 Micropore Capacity, kg/kg	300	155
N_2 Total Capacity, kg/kg	370	260
Particle density ρ_p .10^3, kg/m^3	1.14	
Particle diameter d_p 10^3, m	3.8	

Table 5. Textural properties of the adsorbents studied [Dantas *et al*., 2010].

	Activated carbon	CPHCL
C	86.2	70.2
H	1.3	2.0
N	0.9	1.4
N/C. 10²	1	2

Table 6. Chemical characterization of the adsorbents studied. [Dantas *et al*., 2010].

It has been suggested that primary amine can react with the activated carbon surface, forming surface complexes with the presence of NH_2 surface groups (Gray *et al*., 2004). Bands were presence at 3365 and 1607 cm^{-1}, ascribed to asymmetric stretching (νNH_2) and NH_2 deformation, respectively, and at 3303 cm^{-1}. However, the CPHCL spectrum shows that these bands may be overlapped by the OH stretching band (3600-3100 cm^{-1}) and by the aromatic ring bands and double bond (C=C) vibrations (1650-1500 cm^{-1}) (Fanning & Vannice, 1993). The same pattern is observed for CPHCL after CO_2 adsorption at 28°**C** and 150°**C**, indicating that there is no difference in the adsorption behavior.

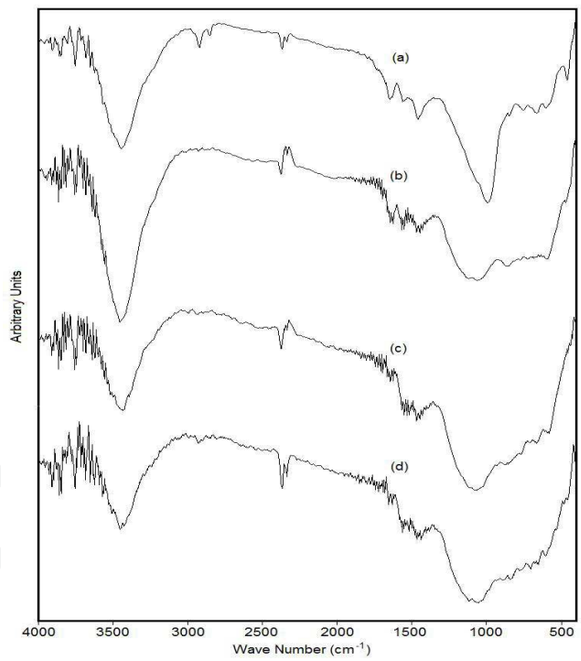

Fig. 1. FTIR spectra of (a) commercial activated carbon; (b) CPHCL; (c) CPHCL after pre-treatment and CO_2 adsorption at 28°**C** and (d) CPHCL after pre-treatment and CO_2 adsorption at 150°**C** [Dantas *et al*., 2010].

4.2 Adsorption equilibrium isotherms

The adsorption equilibrium of CO_2 and N_2 adsorption on activated carbon was previously (Dantas *et al*., 2010) described using the Toth model (Toth, 1971); Eq. (29):

$$q = \frac{q_m K_{eq} P}{\left[1 + (KP)^n\right]^{1/n}} \tag{29}$$

where q_m is the maximum adsorbed concentration, i.e., the monolayer capacity; K_{eq} is the equilibrium adsorption constant and n is the heterogeneity parameter.

The temperature dependence of the equilibrium was described according to the Van't Hoff equation; Eq. (30):

$$K_{eq} = K_o . e^{\left(\frac{-\Delta H_i}{R.T}\right)} \tag{30}$$

where K_o is the adsorption constant at infinite dilution.

Table 7 gives the parameters used for Toth model isotherms of each gas. It should be noted that activated carbon has a high CO_2 adsorption capacity in comparison with the N_2 adsorption capacity. It is worth mentioning that the commercial activated carbon used in this studied has a high CO_2 adsorption capacity in comparison with other adsorbents reported in literature (Grande & Rodrigues, 2008; Glover *et al*., 2008).

The CO_2 adsorption equilibrium isotherms for CPHCL, at low partial pressure, were described according a linear isotherm (Dantas *et al*., 2010); (Eq.31):

$$q = K_p P \tag{31}$$

where K_p is the Henry's Law constant for the adsorption equilibrium which the temperature dependence was also described according to the Van't Hoff equation.

Gas	q_m, 10^{-3}mol/g	*n*	K_o, bar^{-1}	$-\Delta H_i$, kJ/mol
CO_2	*10.05*	*0.68*	*7.62 × 10^{-5}*	*21.84*
N_2	*9.74*	*0.52*	*6.91 × 10^{-5}*	*16.31*

Table 7. Parameters used for fitting of the Toth model for carbon dioxide and nitrogen adsorption o activated carbon.

Table 8 gives the Henry's Law constants for the adsorption equilibrium on CPHCL, at the different temperatures studied, the pre-exponencial factor and heat of adsorption. Table 8 also shows the Henry's constants for the adsorption equilibrium on commercial activated carbon that was fitted at low pressure.

It should be noted, however, that the commercial activated carbon has higher Henry's Law constant indicating that this solid has a greater carbon dioxide adsorption capacity.

The nature of the N functionality is very important because it can affect the basicity of the solid surface (Vlasov & Os'kina, 2002); comparing a primary amine with a secondary amine of the same carbon number, the basic character increases due to the increase in the inductive effect caused by the alkyl groups.

Some authors have reported that although there is a reduction in the BET superficial area which is caused for the partial blockage of the lesser pores, as also observed in this paper, the enrichment of the carbonaceous materials with nitrogen tends to increase the adsorption capacity for CO_2 (Arenillas *et al*., 2005). However, there is no consensus about this issue because sorbents with the high amounts of nitrogen do not have the high CO_2 adsorption capacity reported in recent publications by Arenillas and coworkers (2005) and Pevida *et al*. (2008). In the present study, we show a decrease in the CO_2 adsorption capacity of CPHCL in comparison with non-functionalized activated carbon. The decrease in the CO_2 adsorption capacity is not related to the destruction of basic sites in the CPHCL, as shown in the FTIR studies (Figure 2). In fact, Drage *et al*. (2007) have reported that only an activation temperature higher than 600°C can destroy basic sites in the adsorbents.

	Activated carbon	**CPHCL**	
T, °C	**K_p, moles/kg. bar^{-1}**	**K_p, moles/kg. bar^{-1}**	**$-\Delta H_i$, kJ/mol**
28-25	2.89	2.16	20.25
50	1.86	1.55	
100	0.62	0.32	
150	0.29	0.11	

Table 8. Henry's Law constants for the adsorption equilibrium on commercial activated carbon and CPHCL at different temperatures (Dantas *et al*., 2010).

4.3 Fixed-Bed CO_2 adsorption: experimental data and modeling

As previously mentioned, a set of experiments was performed changing the temperature of the carbon dioxide to determine the breakthrough curves of carbon dioxide adsorption on activated carbon and CPHCL.

The Peclet number and the LDF global mass transfer coefficient for the adsorption of carbon dioxide on activated carbon and CPHCL are shown in Table 9.

Run	**T, °C**	*Pe*	**Activated Carbon** K_L **, s^{-1}**	**CPHCL** K_L **, s^{-1}**
1	*28*	21.91	0.0027	0.0041
2	*50*	21.85	0.0043	0.0063
3	*100*	21.75	0.0125	0.0259
4	*150*	21.65	0.0259	0.0719

Table 9. Experimental Conditions and LDF global mass transfer coefficient for CO_2 adsorption on the commercial activated carbon and CPHCL (Adapted from Dantas *et al*., 2010).

Figures 2(a) e 2(b) shows a comparison between the experimental and theoretical curves obtained for the CO_2 adsorption on commercial activated carbon and CPHCL, respectively.

It is observed that, in the case of the mass balance, the model reproduces the experimental data for the different feed concentration and temperatures reasonably well.

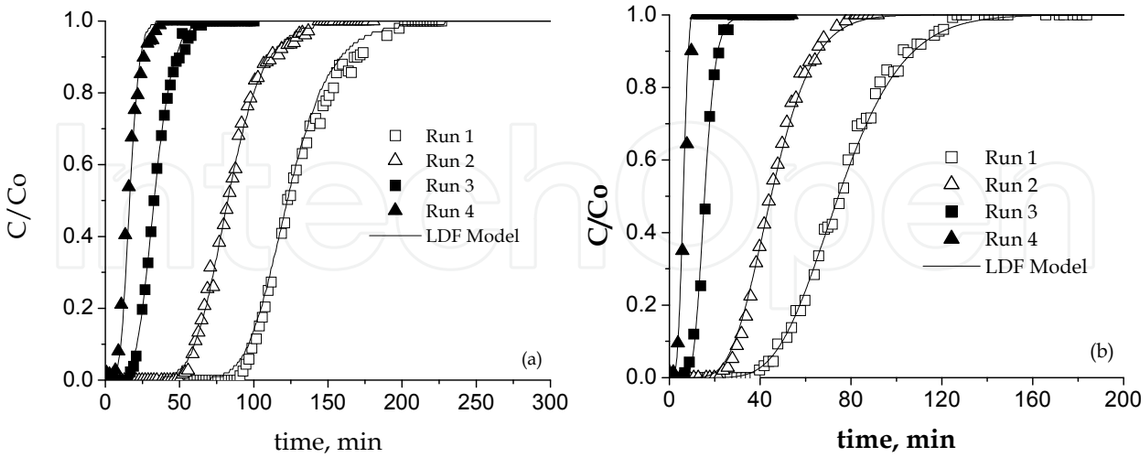

Fig. 2. Breakthrough curves for the CO_2 adsorption (a) on activated carbon and (b) on CPHCL. Symbols: experimental data; Lines: LDF model (Dantas *et al.*, 2010).

The global mass transfer coefficient for CO_2 adsorption on CPHCL in the fixed bed is higher than that for the adsorption on activated carbon (Table 9) which was to be expected because the CPHCL is an adsorbent with less micropores and smaller CO_2 adsorption capacity than the commercial activated carbon. This makes the importance of the external to the internal mass transfer resistance (Eq. (28)) greater in the case of CPHCL than commercial activated carbon.

Figures 3(a) e 3(b) shows the gas simulated temperature profile, at the end of the bed, for the carbon dioxide adsorption at 28°**C** on activated carbon and CPHCL, respectively**.**

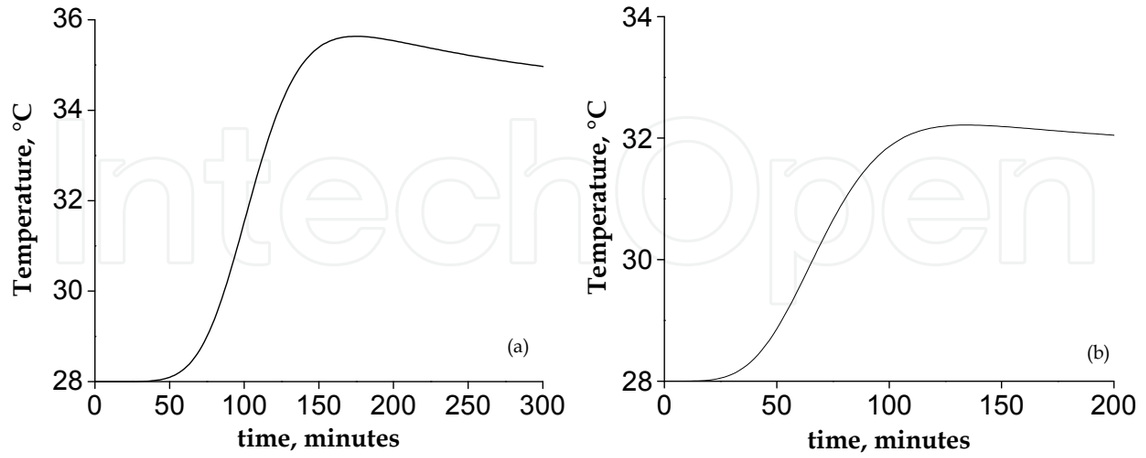

Fig. 3. Gas simulated temperature profile, at the end of the bed, for the carbon dioxide adsorption at 28°C (a) on activated carbon and (b) on CPHCL.

The temperature peaks is about 8°C and 4°C, for activated carbon and CPHCL, respectively. Although as the commercial activated carbon and the CPHCL have about the same heat of

adsorption, but distinct adsorptive capacities, it is also possible to conclude that a higher adsorption capacity leads to a higher temperature peak, since the adsorption is an exothermic phenomenon.

4.4 Fixed-Bed CO_2/N_2 mixture adsorption: Experimental data and modeling

The basic information required to describe the fixed-bed dynamics of the adsorption of carbon dioxide-nitrogen mixtures on activated carbon is the adsorption equilibrium behavior of the single components. The adsorbed equilibrium concentration of carbon dioxide and nitrogen on activated carbon was estimated as a function of the feed concentration from a mass balance in the fixed bed. For each experimental breakthrough curve, the adsorbed concentration is given by:

$$q_i = \frac{1}{\rho_p}\left[\frac{C_{Fi}Q_F t_{st}}{(V-\varepsilon V)} - \frac{C_{Fi}\varepsilon}{(1-\varepsilon)}\right] \tag{32}$$

where *CFi* is the feed concentration of component i, *V* is the bed volume, *QF* is the feed volumetric flow rate and *tst* is the stoichiometric time (Ruthven, 1984).

The resulting adsorbed concentrations are given in Table 10. It can be observed that the activated carbon adsorption capacity for CO_2 and N_2 in the CO_2/N_2 mixtures is the same as that predicted by the single component Toth isotherm using the previously reported adjusted. This is to be expected if the active sites for N_2 and CO_2 are independent, since the amount of CO_2 and/or N_2 adsorbed on the solid at each partial pressure from a CO_2/N_2 mixture is the same as that measured for the pure gases at the same partial pressure, as shown in Table 10. This assumption is in agreement with Siriwardane and coworkers (2001) who observed the same behavior for the adsorption of CO_2/N_2 mixtures on 13X zeolite, although Delgado and coworkers (2006) observed that the nitrogen adsorption can be neglected when it is mixed with carbon dioxide. As the presence of nitrogen in the mixture does not interfere at the CO_2 adsorption on activated carbon, thus the pure component equilibrium isotherms predict very well the equilibrium of each component in the CO_2/N_2 mixture.

Run	T, °C	Adsorbate	*q*, mol kg$^{-1(a)}$	*q*, mol kg$^{-1(b)}$
1	***28***	N_2	0.272	0.294
		CO_2	0.734	0.743
2	***50***	N_2	0.178	0.173
		CO_2	0.450	0.466
3	***100***	N_2	0.097	0.096
		CO_2	0.163	0.170
4	***150***	N_2	0.054	0.059
		CO_2	0.072	0.071

Table 10. Experimental conditions and adsorbed concentrations predicted by the Toth model for pure components and from the mass balance of breakthrough experiments on activated carbon. (a) Values calculated from the experimental data; (b) Values calculated using Toth model for single component adsorption.

As previously mentioned, a set of experiments was performed changing the temperature of the carbon dioxide/nitrogen mixture to determine the breakthrough curves of carbon dioxide adsorption and nitrogen adsorption on activated carbon.The axial mass dispersion coefficient and the LDF global mass transfer coefficient for CO_2 and N_2 adsorption on activated carbon are shown in Table 11.

Run	T, °C	D_L , cm² s⁻¹	CO_2	N_2
			K_L , s⁻¹	
1	*28*	0.10	0.0025	0.004
2	*50*	0.10	0.0042	0.011
3	*100*	0.10	0.0138	0.042
4	*150*	0.10	0.0323	0.128

Table 11. Axial mass dispersion coefficient and the LDF global mass transfer coefficient for CO_2 and N_2 adsorption on activated carbon (Adapted from Dantas *et al*., 2011).

Figure 4 shows a comparison between the experimental and theoretical curves obtained for the N_2 and CO_2 adsorption on activated carbon. The model describes quite well the roll-up effect that is caused by the displacement of N_2 by CO_2 (Dabrowski, 1999). The roll-up is a common phenomenon happening in multicomponent adsorption processes when the concentration of one component at outlet of the adsorber exceed it inlet level (Li et al., 2011). It can be observed that, when the temperature is increased, the carbon dioxide and nitrogen breakthrough times are shorter due the exothermic character of adsorption.

The nitrogen breakthrough times are very similar at 28°**C** and 150°**C**. This finding can be explained by the decrease in the amount of nitrogen adsorbed on activated carbon which can be compensated by its faster diffusion at high temperature as observed by Cavenati and coworkers (2006) for nitrogen adsorption on CMS 3K (as mentioned above, this molecular sieve has a similar pore size distribution to that used for the activated carbon in this study). The model reproduces very well the breakthrough curves for the different feed concentrations, including the experimental breakthrough curves obtained for nitrogen. Also, from the breakthrough curves we can note that the adsorbent is very selective towards carbon dioxide.

4.5 PSA: Experimental data and modeling

Figure 5 shows the pressure change as a function of the process time for the experimental conditions of Run 1 (see Table 2). A function was not found to describe with more accuracy the pressure drop during the blowdown step and therefore the model cannot predict very well this process variable.

Figure 6 shows the experimental and simulated changes for CO_2 molar flow rate during the PSA separation. The solid line represents the first cycle and the dashed line the steady-state cycle (CCS).

Figure 7 shows the experimental and simulated N_2 molar flow rate as a function of process time, under the experimental conditions of run 2. The assumption that nitrogen adsorption does not affect the CO_2 adsorption is well represented by the simulation, since the flow rate of nitrogen is not modified during each step.

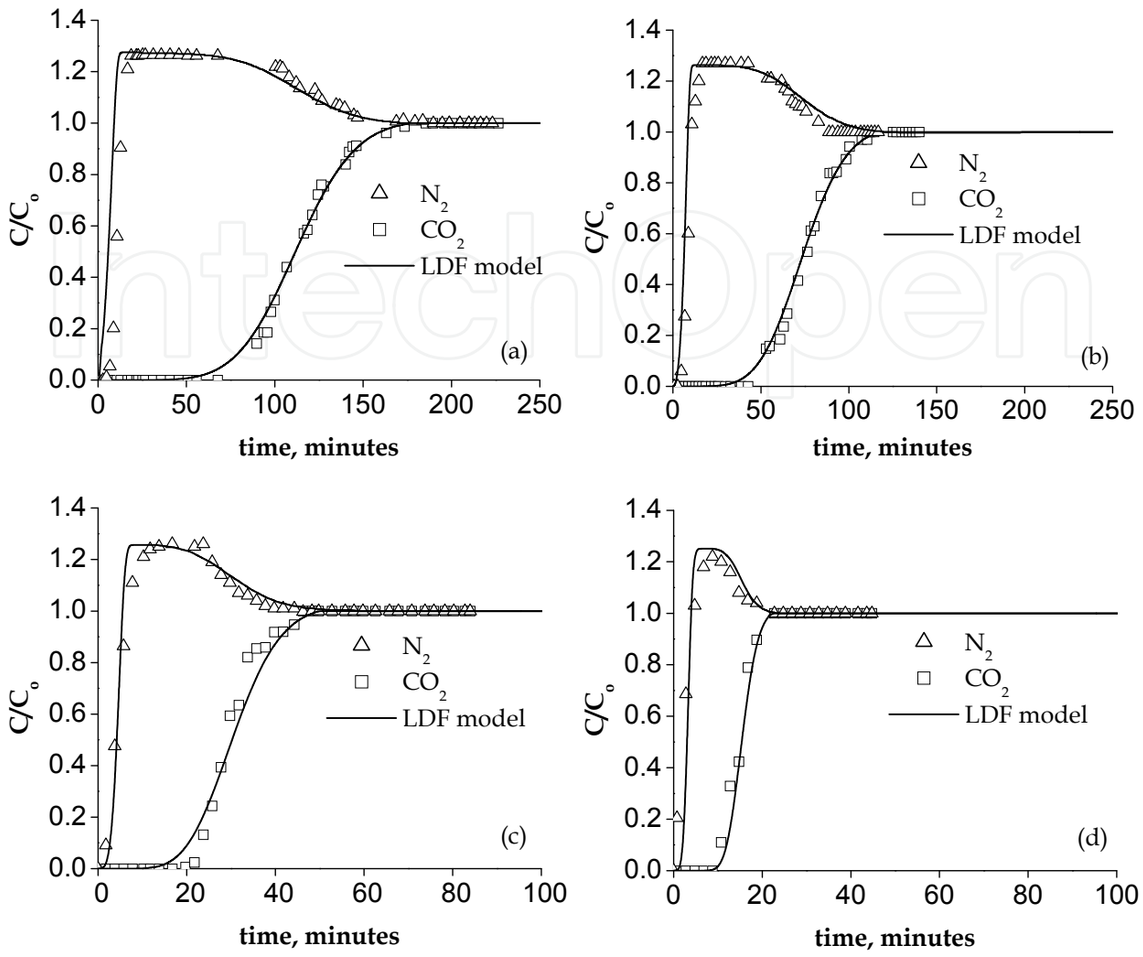

Fig. 4. Breakthrough curves for the N_2 and CO_2 adsorption on commercial activated carbon. Symbols: experimental data; Δ N_2 and □ CO_2. Lines: LDF model. Conditions: (a) run 1; (b) run 2; (c) run 3; and (d) run 4.

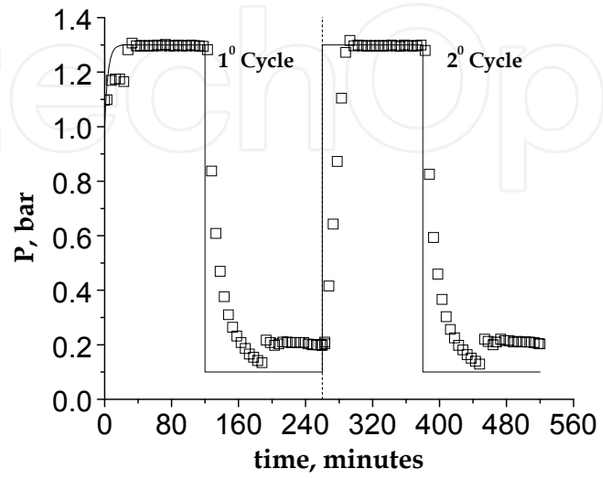

Fig. 5. Pressure change as a function of process time. Experimental conditions: run 1.

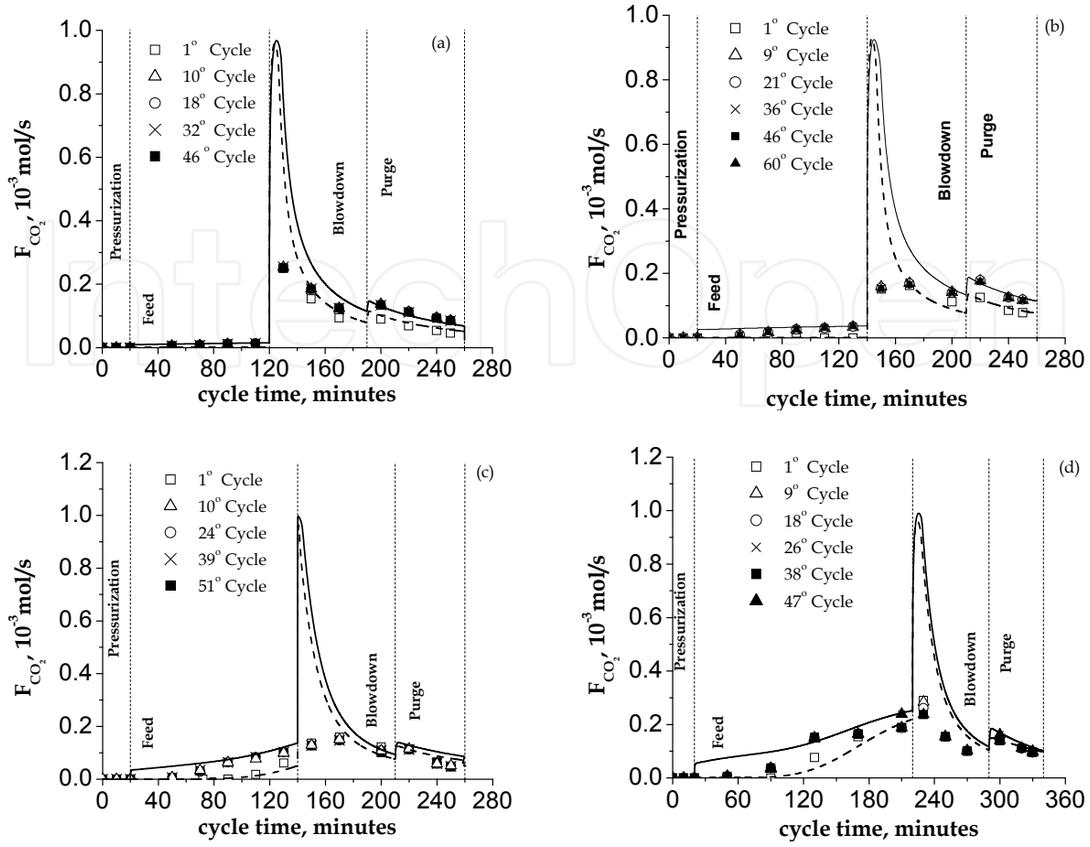

Fig. 6. Carbon dioxide molar flow rate as a function of cycle time. Experimental conditions: (a) run 1; (b) run 2; (c) run 3; and (d) run 4. Solid line: first cycle simulation. Dashed line: CCS simulation.

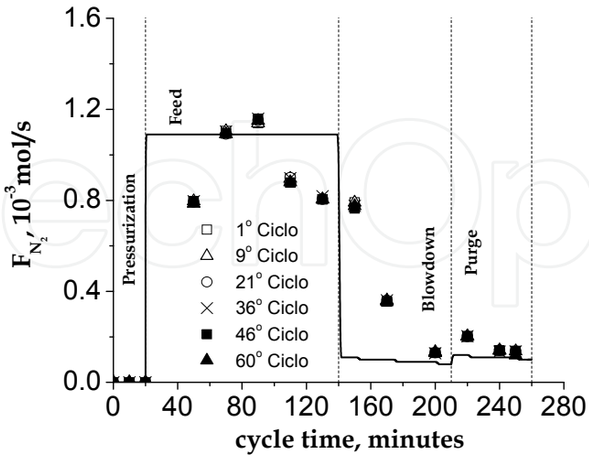

Fig. 7. Nitrogen molar flow rate as a function of cycle time. Experimental conditions: run 2. Solid line: first cycle simulation. Dashed line: CCS simulation.

Figures 8(a) and 8(b) shows the experimental and simulated temperature profile inside the column, at 0.17 m and 0.43 m from the bottom of the column, under the experimental

conditions of run 3. The temperature peak is high due to the exothermic adsorption of CO_2 on activated carbon in a high amount. Therefore heat effects cannot be neglected during adsorption, especially when there is a strong adsorbent-adsorbate interaction.

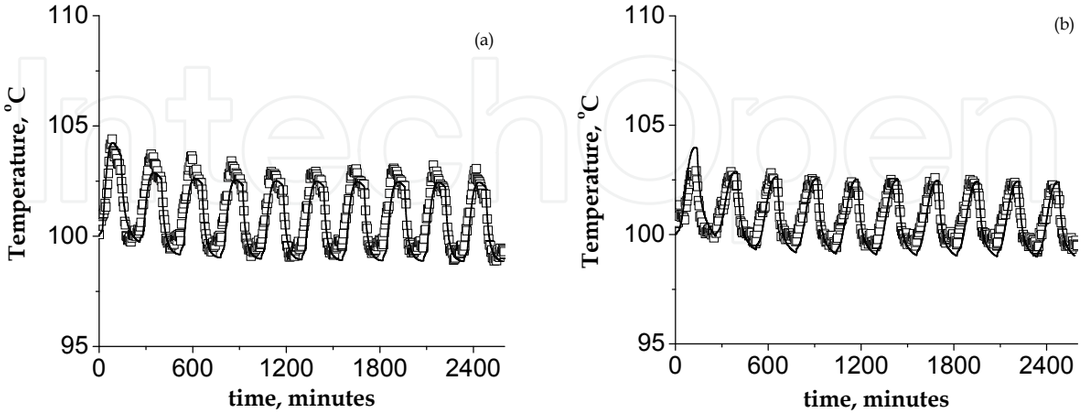

Fig. 8. Temperature profile of the gas phase: (a) at 0.17 m and (b) at 0.43 m from the bottom of the column. Experimental conditions: run 3.

Table 12 shows the performance of the PSA process: carbon dioxide recovery, nitrogen recovery, and carbon dioxide purity obtained for all experimental conditions studied. It is possible note that there is an increase in the carbon dioxide purity with increasing feed time (runs 1 and 2). This indicates that the separation is strongly controlled by the equilibrium. It can be also noted that there is an increase in the carbon dioxide purity with increasing temperature and this is due to the high selectivity of activated carbon. We observed that when the temperature of the CO_2/N_2 mixture was 100°C, a superior CO_2 purity is obtained due to the high selective toward CO_2. This is a good result since it indicates that the cooling of the exhaustion gas before CO_2 separation is not necessary.

Run	Feed time, s	CO_2 purity, %	N_2 purity, %	CO_2 recovery, %
1	100	25.7	87.1	93.1
2	120	31.3	87.5	85.4
3	120	32.3	87.1	73.7
4	200	49.7	78.9	66.8

Table 12. PSA Performance.

As proposed by Grande and Rodrigues (2008) for CO_2 adsorption, adsorbents with a greater adsorption capacity and higher heat of adsorption than the activated carbon honeycomb monolith should be used to achieve a product purity of greater than 16%. Although the CO_2 purity is lower than that is required to transport, the PSA cycle could be optimized in order to increase the CO_2 purity and recovery (Ko *et al.*, 2005). Transport considerations limit the CO_2 purity > 95.5% to ensure a reasonable input of CO_2 compression power (Vinay & Handal, 2010).

5. Conclusion

There are many factors that influence CO_2 capture, some of them are physical and some chemical. Textural properties are important for any adsorption processes but, in the case of CO_2 capture, the surface chemistry is a particularly important factor. The enrichment of activated carbon with nitrogen using amine 3-chloropropylamine hydrochloride blocked some pores of the activated carbon. The increase in the surface basicity was not sufficient to counteract the decrease in the BET superficial area since a reduction in the CO_2 adsorption was observed.

Carbon dioxide adsorption on commercial activated carbon and on a nitrogen-enriched activated carbon, named CPHCL, packed in a fixed bed was studied. The adsorption equilibrium data for carbon dioxide on the commercial activated carbon were fitted well using the Toth model equation, whereas for carbon dioxide adsorption on the CPHCL a linear isotherm was considered. A model using the LDF approximation for the mass transfer, taking into account the energy balance, described the breakthrough curves of carbon dioxide adequately. The LDF global mass transfer coefficient for the adsorption of CO_2 on activated carbon is smaller than that for the CPHCL. Since part of the micropores of the activated carbon are blocked by the incorporation of the amine, probably only the largest pores would be filled by the CO_2, causing a decrease on the capacity of the adsorption and an increase on the adsorption rate.

The fixed-bed adsorption of CO_2/N_2 mixtures on activated carbon was also studied. The adsorption dynamics was investigated at several temperatures and considering the effects caused by N_2 adsorption. It was demonstrated that the solid sorbent adsorbed carbon dioxide and nitrogen to its total capacity, leading to the conclusion that the equilibrium of CO_2 and N_2 adsorption from CO_2/N_2 mixtures could be very well described through the adsorption equilibrium behavior of the single components. The activated carbon used in this study has high selectivity for CO_2 and is suitable for CO_2/N_2 separation processes. The model proposed herein can be used to design a PSA cycle to separate the components of CO_2/N_2 mixtures, where the pressure drop and thermal effects are very important.

The carbon dioxide–nitrogen separation applying PSA process showed that the increase in the inlet temperature of the mixture CO_2/N_2 increases the CO_2 purity due to the great difference between the adsorption capacities of N_2 and CO_2.

6. Acknowledgments

The authors are grateful to CAPES – Comissão de Aperfeiçoamento de Pessoal de Nível Superior (Brazil) – and to CAPES/GRICES for the International Cooperation Project (Brazil/Portugal)

7. References

Arenillas, A.; Rubiera, F; Parra, J.B.; Ania, C.O. & Pis, J.J. (2005). Surface modification of low costs carbons for their application in the environmental protection. *Applied Surface Science*, 252, Vol.252, No.3, pp. 619-624, ISSN 0169-4332.

Bird, R.B.; Stewart, W.E. & Lightfoot, E.H. (2007). Transport Phenomena. Wiley, New York, 2nd Edition, ISBN 0471410772.

Brunauer, S.; Emmett, P.H. & Teller, E. (1938). Adsorption of Gases in Multimolecular Layers. *Journal of American Chemical Society*, Vol. 60, No.2, pp. 309-319, ISSN 00027863.

Cavenati, S.; Grande, C.A. & Rodrigues, A.E. (2006). Separation of $CH_4/CO_2/N_2$ mixtures by layered pressure swing adsorption for upgrade of natural gas. *Chemical Engineering Science,* Vol.61, No.12, pp. 3893-3906, ISSN 0009-2509.

Dabrowski, A. Adsorption and its applications in industry and environmental protection, Vol I. Applications in industry (1999). Elsevier Science, ISBN 044450165-7, Netherlands.

Dantas, T.L.P.; Amorim, S.M.; Luna, F.M.T.; Silva Junior, I. J.; Azevedo, D.; Rodrigues, A. E.; Moreira, R.F.P.M. (2010). Adsorption of carbon dioxide onto activated carbon and nitrogen-enriched activated carbon: Surface Changes, Equilibrium, and Modeling of Fixed-Bed Adsorption. *Separation Science and Technology*, Vol.45, No.1, pp.73 - 84, ISSN 1383-5866.

Dantas, T.L.P.; Amorim, S.M.; Luna, F.M.T.; Silva Junior, I. J.; Azevedo, D.; Rodrigues, A. E.; Moreira, R.F.P.M. (2011). Carbon dioxide-nitrogen separation through adsorption on activated carbon in a fixed bed. *Chemical Engineering Journal*, Vol. 172, No.2-3, pp.698 - 704, 2010, ISSN 1385-8947.

Da Silva, F. A. & Rodrigues, A.E. (2001). Propylene/Propane separation by vacuum swing adsorption using 13X zeolite. *AIChE Journal*,Vol.47, No.2, pp. 341-357, ISSN 1547-5905.

De Boer, J. H.; Lippens, B. C.; Lippens, B.G.; Broekhoff, J.C.P.; Van den Heuvel, A. & Osinga, Th. J. (1966). The T-Curve of Multimolecular N_2-adsorption. *Journal of Colloid and Interface Science*, Vol.21, No.4, pp. 405-414, ISSN 0021-9797.

Delgado, J.A.; Uguina, M.A.; Gómez, J.M; Sotelo, J.L. & Ruíz, B. (2006). Fixed-bed adsorption of carbon dioxide-helium, nitrogen-helium and carbon dioxide-nitrogen mixtures onto silicalite pellets. *Separation and Purification Technology*, Vol.49,No.1, pp. 91-100, ISSN 1383-5866.

De Wash, A.P. & Froment, G. (1972). Heat transfer in packed beds. *Chemical Engineering Science*, Vol.27, No.3, pp. 567-576, ISSN 0009-2509.

Drage, T.C.; Arenillas, A.; Smith, K.M.; Pevida, C.; Piipo, S. & Snape, C.E. Preparation of carbon dioxide adsorbents from the chemical activation of urea-formaldehyde and melamine-formaldehyde resins. *Fuel*, Vol.86, No.1-2, pp.22-31, ISSN 0016-2361.

Dubinin, M.M. & Radushkevich. L.V. (1947). *Proc. Acad. Sci. Phys. Chem. Sec. USSR*, Vol.55, pp. 331.

Fanning, P.E. & Vannice, M.A. (1993). A drift study of the formation of surface groups on carbon by oxidation. *Carbon*, Vol.31, No.5, pp. 721-730, ISSN 0008-6223.

Farooq, S. & Ruthven, D.M. (1990). Heat Effects in Adsorption Column Dynamics. 2. Experimental Validation of the One-dimensional Model. *Industrial & Engineering Chemical Research*, Vol. 29,No.6, pp. 1084-1090, ISSN 0888-5885.

Grande, C.A. & Rodrigues, A. E.(2008). Electric Swing Adsorption for CO_2 removal from flue gases. *International Journal of Greenhouse Gas Control*, Vol.2, No.2, pp. 194-202, ISSN 17505836.

Grant Glover, T.; Dunne, K I.; Davis, R.J. & LeVan, M.D. (2008). Carbon-silica composite adsorbent: Characterization and adsorption of light gases. *Microporous Mesoporous Materials*, Vol.11, No.1-3, pp. 1-11, ISSN 1387-1811.

Gray, M.L.; Soong, Y.; Champagne, K.J.; Baltrus, J.; Stevens Jr, R.W.; Toochinda, P. & Chuang, S.S.C. (2004). CO_2 capture by amine-enriched fly ash carbon sorbents. *Separation and Purification Technology*, Vol. 35, No.1, pp. 31-36, ISSN 13835866.

Ko, D.; Siriwardane, R. & Biegler, L.T. (2005). Optimization of pressure swing adsorption and fractionated vaccum swing adsorption pressure for CO_2 capture. *Industrial & Engineering Chemistry Research*, Vol.44, No. 21, pp. 8084-8094, ISSN 0888-5885.

Leitão, A. & Rodrigues, A.E. (1995). The simulation of solid-liquid adsorption in activated carbon columns using estimates of intraparticle kinetic parameters obtained from continuous stirred tank reactor experiments. *The Chemical Engineering Journal*, Vol.58, No.3, pp. 239-244, ISSN 1385-8947.

Li, G.; Xiao, P.; Xu, D.; Webley, P. A. (2011). Dual mode roll-up effect in multicomponent non-isothermal adsorption processes with multilayered bed packing. *Chemical Engineering Science*, Vol.66, No. 6, pp- 1825-1834, ISSN: 0009-2509.

Mulgundmath ,V. & Tezel ,F.H. (2010). Optimisation of carbon dioxide recovery from flue gas in a TPSA system. *Adsorption*, Vol.16, No.6, pp. 587-598, ISSN 1572-8757.

Pevida, C.; Plaza, M.G.; Arias, B.; Fermoso, J.; Rubiera, F. & PIS, J.J. (2008). Surface modification of activated carbons for CO_2 capture. *Applied Surface Science*, Vol.254, No.2, pp. 7165-7172, 2008, ISSN 0169-4332.

Ruthven, D. M. (1984). Principles of Adsorption and Adsorption Processes. John Wiley & Sons, ISBN 0-471-86606-7.

Siriwardane, R.V.; Shen, M-S. & Fisher, E.P. (2001). Adsorption of CO_2 on Molecular Sieves and Activated Carbon. *Energy Fuels*, Vol.15, No.2, pp. 279-284, ISSN 0887-0624.

Sivakumar, S.V. & Rao, D.P. (2011). Modified duplex PSA. 1. Sharp separation and process intensification for CO_2-N_2-13 X zeolite system. *Industrial & Engineering Chemistry Research*, Vol.50, No.6, pp. 3426-3436, ISSN 0888-5885.

Vinay, M. & Handal, T. (2010). Optimisation of carbon dioxide recovery from flue gas in TPSA system. *Adsorption*, Vol.16, No.6, pp. 587-598, ISSN 1572-8757.

Vinu, A. & Hartmann, M. (2005). Characterization and microporosity analysis of mesoporous carbon molecular sieves by nitrogen and organics adsorption. *Catalysis Today*, Vol.102-103, (May 2005), pp. 189-196, ISSN 0920-5861.

Wakao, N. & Funazkri.T. (1978). Effect of fluid dispersion coefficients on particle-to-fluid mass transfer coefficients in packed beds: Correlation of Sherwood numbers. *Chemical Engineering Science*, Vol. 33,No.10, pp. 1375-1384, ISSN 0009-2509.

Wakao, N.; Kaguei, S. & Nagai, H. (1978). Effective diffusion coefficients for fluid species reacting with first order kinetics in packed bed reactors and discussion on evaluation of catalyst effectiveness factors. *Chemical Engineering Science*, Vol. 33, No.2, p. 183-187, ISSN 0009-2509.

Zhang, J.; Webley, P.A. & Xiao, P. (2008). Effect of process parameters on power requirements of vacuum swing adsorption technology for CO_2 capture from flue gas. *Energy Conversion and Management*, Vol.49, No.2, pp. 346-356, ISSN 0196-8904.

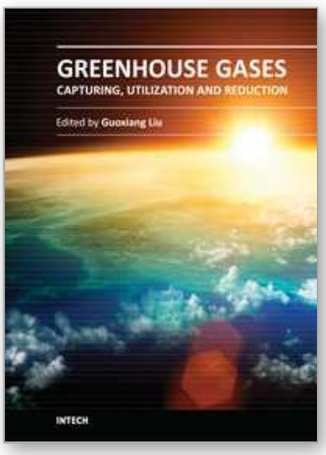

Greenhouse Gases - Capturing, Utilization and Reduction
Edited by Dr Guoxiang Liu

ISBN 978-953-51-0192-5
Hard cover, 338 pages
Publisher InTech
Published online 09, March, 2012
Published in print edition March, 2012

Understanding greenhouse gas capture, utilization, reduction, and storage is essential for solving issues such as global warming and climate change that result from greenhouse gas. Taking advantage of the authors' experience in greenhouse gases, this book discusses an overview of recently developed techniques, methods, and strategies: - Novel techniques and methods on greenhouse gas capture by physical adsorption and separation, chemical structural reconstruction, and biological utilization. - Systemic discussions on greenhouse gas reduction by policy conduction, mitigation strategies, and alternative energy sources. - A comprehensive review of geological storage monitoring technologies.

How to reference
In order to correctly reference this scholarly work, feel free to copy and paste the following:

Tirzhá L. P. Dantas, Alírio E. Rodrigues and Regina F. P. M. Moreira (2012). Separation of Carbon Dioxide from Flue Gas Using Adsorption on Porous Solids, Greenhouse Gases - Capturing, Utilization and Reduction, Dr Guoxiang Liu (Ed.), ISBN: 978-953-51-0192-5, InTech, Available from: http://www.intechopen.com/books/greenhouse-gases-capturing-utilization-and-reduction/separation-of-carbon-dioxide-from-flue-gas-using-adsorption-on-porous-solids

INTECH
open science | open minds

InTech Europe
University Campus STeP Ri
Slavka Krautzeka 83/A
51000 Rijeka, Croatia
Phone: +385 (51) 770 447
Fax: +385 (51) 686 166
www.intechopen.com

InTech China
Unit 405, Office Block, Hotel Equatorial Shanghai
No.65, Yan An Road (West), Shanghai, 200040, China
中国上海市延安西路65号上海国际贵都大饭店办公楼405单元
Phone: +86-21-62489820
Fax: +86-21-62489821

IntechOpen